# Correlation of nanostructural parameters and macromechanical behaviour of hyperbranched-modified polypropylene using time-resolved small-angle X-ray scattering measurements. Polym...

**ARTICLE** *in* POLYMER INTERNATIONAL · OCTOBER 2012

Impact Factor: 2.41 · DOI: 10.1002/pi.4399

Research Article

Received: 22 May 2012 Revised: 25 July 2012 Accepted: 15 August 2012 Published online in Wiley Online Library: 30 October 2012

(wileyonlinelibrary.com) DOI 10.1002/pi.4399

# Correlation of nanostructural parameters and macromechanical behaviour of hyperbranched-modified polypropylene using time-resolved small-angle X-ray scattering measurements

**Morteza Ganjaee Sari,[a] Norbert Stribeck,[b] Siamak Moradian,[c,d] Ahmad Zeinolebadi,[b] Saeed Bastani[d,e]* and Stephan Botta[f]**

## Abstract

**Polypropylene (PP) is modified utilizing a poly(ester amide)-based hyperbranched polymer (PS). A maleic-modified PP is used to enhance the compatibility. Usual tensile experiments are carried out. The nanocrystalline structure is studied using small-angle X-ray scattering (SAXS) while a uniaxial mechanical load is simultaneously applied. SAXS patterns are analysed using procedures written in PV-WAVE. The chord distribution function (CDF) is calculated and nanostructural parameters such as long period ($l_p$) and nanodeformation ($\varepsilon_{Nano}$) are extracted. The correlations between macromechanical parameters and nanostructures are studied. Mechanical results show that PS has a plasticizing effect. Reactively blended samples demonstrate enhanced mechanical properties. SAXS patterns reveal a well-known structure of PP as a peculiar architecture of the nanostructure. Crystalline branching occurs in a geometry that is known as a mother–daughter crystal lamellar structure, also called a crosshatching structure. It is concluded that adding PS distorts the stacking of crystalline domains. The structural information from SAXS patterns in reciprocal space is visualized in real space in the calculated CDFs. The CDFs indicate that in simple blends, $l_p$ of the crystalline stacks increases compared to blank PP. Nevertheless, reactively blended samples show an increase of $l_p$ compared to blank PP; however, they possess smaller $l_p$ compared to simple blends.**


**Keywords:** polypropylene; hyperbranched; nanostructures; mechanical properties; SAXS

## INTRODUCTION

Polypropylene (PP) fibres are not usually regarded as textile fibres, although they show favourable physical and mechanical properties.[1–10] The reason is their lack of dyeability. Many efforts have been made to improve the dyeability.[11–18] One of the most recent approaches is the modification of PP by incorporation of dendritic molecules using either physical or reactive blending.[1,19,20] After having prepared such materials, it is necessary to investigate the effect of the modification on their mechanical properties. It is a matter of great importance that the advantageous mechanical characteristics of PP remain unchanged or are improved. Apparently, variations in macromechanical behaviour of the modified PP can be determined using tensile measurements. However, to gain a better understanding of the mechanisms that govern this behaviour, it appears reasonable to monitor the nanostructural parameters of the polymer. The properties depend on the semi-crystalline morphology. In contrast to most polymers, PP is inclined to form a crosshatched structure in which daughter lamellae interconnect the main or mother lamellae, thus forming a three-dimensional (3D) scaffold that strengthens the polymer.[21–24] An aim of the present investigation was also to track the effects of hyperbranched polymer on such nanostructure. This can lead to a clearer perception of how the modified PP responds to mechanical loads and why it shows a peculiar behaviour in its mechanical properties.

* *Correspondence to: Saeed Bastani, Center of Excellence for Color Science and Technology, Institute for Color Science and Technology, PO 16688-14811, Tehran, Iran. E-mail: bastani@icrc.ac.ir*

a *Department of Nanomaterials and Nanocoatings, Institute for Color Science and Technology, PO 16765-654, Tehran, Iran*

b *Institute TMC, Department of Chemistry, Hamburg University, Hamburg, Germany*

c *Department of Polymer Engineering and Color Technology, Amirkabir University of Technology, PO 15875-4413, Tehran, Iran*

d *Center of Excellence for Color Science and Technology, Institute for Color Science and Technology, PO 16688-14811, Tehran, Iran*

e *Department of Surface Coating and Corrosion, Institute for Color Science and Technology, PO 16765-654, Tehran, Iran*

f *HASYLAB at DESY, Notkestr. 85, 22603, Hamburg, Germany*

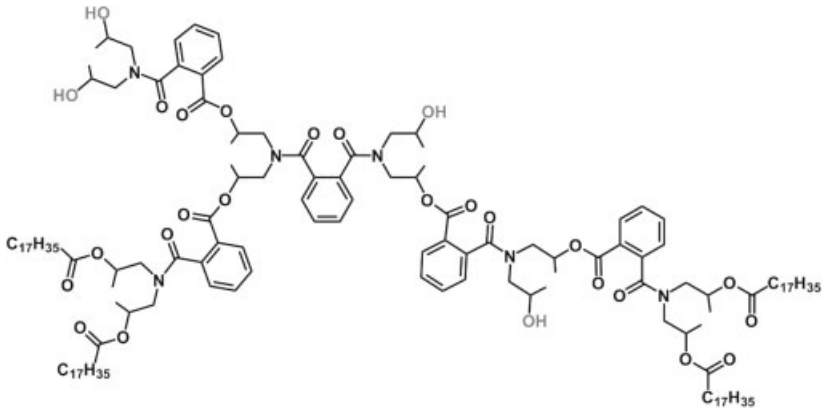

**Figure 1.** Structure of DSM Hybrane PS2550.

One of the most versatile methods by which an accurate and precise quantitative study of the structural evolution and nanostructural parameters during deformation can be carried out is X-ray scattering.[21,25] Because of developments in synchrotrons and detectors, nowadays the required exposure time to obtain a low-noise scattering pattern has significantly decreased. It has made measurements possible in a time-resolved mode during mechanical tests instead of stepwise evaluations in which one had to stop the deformation and expose the sample for a relatively long time during which undesired structural changes were probable. The benefit of such a new technique is that now it is conceivable to expose the sample without stopping the extensometer and gaining a real-time low-noise pattern with minimal changes in structure.[26] Moreover, it is now possible to exploit a method in which a complete scattering pattern in reciprocal space is transformed into a pattern in real space that is a representation of a polymer nanostructure.[27] Model independency and the ability to extract quantitative structural parameters are the advantages of this technique.

The main objective of the work reported in this paper, in which fibre-grade PP was modified utilizing a poly(ester amide)-based hyperbranched polymer, was to study the nanostructure of the hyperbranched-modified PP and its correlation with macromechanical behaviour. Maleic anhydride-modified PP was also used as a coupling agent to simultaneously transform relatively hydrophilic hyperbranched end groups into hydrophobic ones and to bond the hyperbranched polymer to PP chains. The method has been explained in detail elsewhere.[1]

## EXPERIMENTAL

### Materials

PP (V30S, $M_w$: 226 000 g mol$^{-1}$; $M_n$: 55 000 g mol$^{-1}$; polydispersity index: 4.14; melt flow index: 18 g (10 min)$^{-1}$ at 230 °C/2.16 kg) was purchased from Arak Petrochemical Company. The material was stabilized against oxidation and thermal degradation using additives to prevent any undesired change in molecular weight during mixing and injection-moulding processes. A hyperbranched polymer based on poly(ester amide) (PS; Hybrane PS2550, $M_w$ = 2500 g mol$^{-1}$), possessing both hydrophobic stearic acid ester and hydrophilic hydroxyl end groups, was kindly supplied by DSM Hybrane Company. Figure 1 shows the structure of this polymer. PP chemically modified with maleic anhydride (PM) was obtained from DuPont Packaging and Industrial Polymers Company (Fusabond® P MD353D).

**Table 1.** Studied samples and their compositions (wt%)

| Sample | Composition | | |
|---|---|---|---|
| | PP | PS | PM |
| PP | 100 | 0 | 0 |
| PP/PS (95:5) | 90 | 5 | 0 |
| PP/PS (90:10) | 90 | 10 | 0 |
| PP/PS (80:20) | 80 | 20 | 0 |
| PP/PS/PM (90:5:5) | 90 | 5 | 5 |
| PP/PS/PM (80:10:10) | 80 | 10 | 10 |

To blend the materials, a Brabender model W50 Plasticorder internal mixer equipped with a Banbury-type rotor design was used. Blending temperature was kept at 200 °C and the rotor speed was adjusted to 100 rpm. Blending was continued until the rotor torque reached a constant value plus an additional time of approximately 2 min. The overall duration of the mixing process was around 10 min. After discharging the material, it was broken into small pieces using a breaker miller in order to prepare for the subsequent injection-moulding process of tensile bars (dog-bone shape, size S3 according to DIN 53504, thickness 1 mm). The moulding was carried out with a Haake MiniJet piston injection moulding system. The temperatures of the feeding cylinder and the mould were adjusted to 200 and 50 °C, respectively. Piston pressure and back pressure were respectively set at 200 and 170 bar (20 and 17 MPa). Table 1 gives the compositions of the prepared blends.

### Nomenclature

The samples were designated according to their components and their quantities, respectively, separated with slashes and colons (e.g. the sample designated as PP/PS/PM (90:5:5) contains 90 wt% of PP, 5 wt% of PS and 5 wt% of PM).

### Morphology

A Philips XL30 SEM instrument was used to study the morphology of the samples. The samples underwent microtomy at −70 °C using a 45° glass blade. They were then etched for 2 min in a $KMnO_4$ solution (10 mL of $H_2SO_4$ (96–98%), 1 mL of $H_2O$, 0.108 g of $KMnO_4$) and sputtered with around 2 nm of Pt/Pd prior to investigation.



  

### Laboratory tensile tests

The macromechanical properties of the samples were studied before synchrotron measurements utilizing a Zwicki Z1.0/TH1S (Zwick GmbH, Ulm, Germany) extensometer. The experiments were carried out at a rate of 5 mm $min^{-1}$. Every test was repeated five times.

### Small-angle X-ray scattering (SAXS) measurements

SAXS measurements were performed at synchrotron beamline A2 at HASYLAB, Hamburg, Germany. The wavelength of the X-ray beam was 0.15 nm and the sample–detector distance was 2556 mm. Scattering patterns were collected using a two-dimensional (2D) position-sensitive marccd 165 detector (Marresearch, Norderstedt, Germany) operated in 2048 × 2048 pixel mode (pixel size: 79 × 79 $\mu m^2$).

### Tensile testing at beamlines

Tensile testing at the beamlines was carried out with a self-made extensometer[25] adapted for application at HASYLAB beamlines. A 500 N load cell was utilized. The machine applied symmetric drawing and signals from load cell and transducer were then recorded during the experiment. Before fixing the sample in the clamps, some fiducial marks were stamped on the sample to make it possible to calculate the strain in the vicinity of the beam position (Fig. 2(b)).[28] The sample was monitored with a TV camera, and video frames were recorded and stored every 10 s together with the experimental data automatically. In all experiments the machine was operating at velocity of 0.5 mm $min^{-1}$ (Fig. 2(a)). The true elongation $\varepsilon = (l - l_0)/l$ was calculated automatically from the initial distance, $l_0$, of the two fiducial marks enclosing the point of beam irradiation and the respective actual distance, $l$.[29] Also the true stress, $\sigma = F/A$, was calculated from the force obtained by the load cell after deducting the force applied by the upper sample. The actual cross-sectional area, $A = A_0/(1 + \varepsilon)$, was estimated assuming constant volume. $A_0$ is the initial cross-sectional area of the test bars.[21] Scattering patterns were recorded every 30 s with an exposure time of 50 s in multi-read mode. The patterns were normalized and background corrected.[26] This included intensity normalization for constant initial beam flux, zero absorption and constant irradiated volume, $V_0$. The irradiated volume change during the tensile test was corrected considering $V(t)/V_0 = [1/(1 + \varepsilon(t))]^{0.5}$.[21]

For every SAXS pattern that was recorded, several video images were captured and stored together with the elapsed time.

### SAXS data evaluation

To evaluate SAXS data, a model-independent approach was used. In this approach, the scattering patterns in reciprocal space were transformed into a representation of the nanostructure utilizing Fourier transformation.[27] The outcome of such transformation is a multi-dimensional chord distribution function (CDF), $z(\mathbf{r})$.[30] The only assumption is the existence of multi-phase topology. The method has been explained and exemplified by Stribeck and co-workers.[31–38] The method aims to extract the topological information on nanostructure (e.g. a two-phase crystalline–amorphous topology, $\rho(\mathbf{r}) \in [\rho_{cryst}, \rho_{amorph}]$, in which phases with distinct densities are present) from 2D SAXS patterns with uniaxial symmetry. The obtained CDF is an 'edge-enhanced autocorrelation function',[39–42] the autocorrelation of the gradient field, $\nabla\rho(\mathbf{r})$. Thus, as a function of ghost displacement, $\mathbf{r}$, the multi-dimensional CDF, $z(\mathbf{r})$, shows peaks wherever there are domain surface contacts between domains in $\rho(\mathbf{r})$ and in its displaced ghost. The CDF with fibre symmetry in real space, $z(r_{12}, r_3)$, is computed from the fibre-symmetrical SAXS pattern, $I(s_{12}, s_3)$, of multi-phase materials.[10] Vector $\mathbf{s} = (s_{12}, s_3)$ is the scattering vector with its modulus defined by $|\mathbf{s}| = s = (2/\lambda)\sin\theta$. Here $\lambda$ is the wavelength of radiation and $2\theta$ is the scattering angle. In the historical context, the CDF is an extension of Ruland's interface distribution function[43] in the multi-dimensional case or, in a different view, the Laplacian of Vonk's multi-dimensional correlation function.[44]

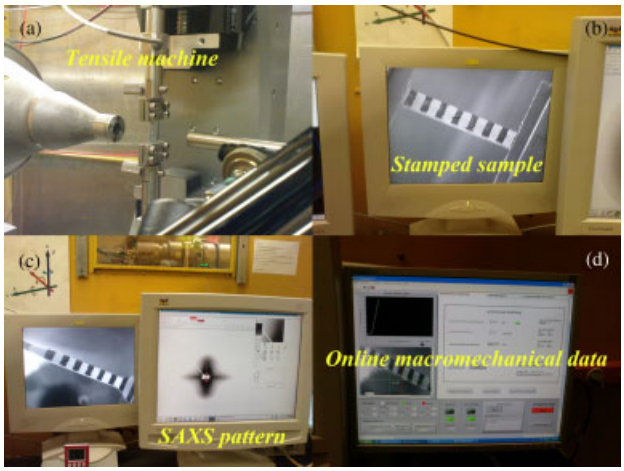


**Figure 2.** Mechanical testing in progress at HASYLAB as observed on monitors. (a) Extensometer fit at beamline. (b) Sample with fiducial marks. The area of X-ray irradiation is marked by an encircled crosshair. (c) Actual SAXS pattern. (d) Mechanical progress (force *versus* machine strain) shown in programming window.

## RESULTS AND DISCUSSION

### Morphology

SEM images of PP, PP/PS (95:5) and PP/PS/PM (90:5:5) are shown in Fig. 3. As expected, PP shows no distinguishable phases. PP/PS (95:5) shows distinctive phase separation. The visible cavities are places where the hyperbranched polymers were situated. Clearly, the cavities retain their shape after extracting the dendritic domains and are not deformed. Phase separation for PP/PS/PM (90:5:5) occurs as smaller domains. Because of the compatibilization that goes along with the mixing of the PS/PM, the domains are smaller and appear more evenly distributed in the PP matrix compared to PP/PS (95:5). Because the volume fraction of the filler is double in PP/PS/PM (90:5:5), in the images the volume fraction of the holes appears to be greater in Fig. 3(c) than in Fig. 3(b). The cavities appear to be deformed after etching. The latter may indicate that a crosslinked hyperbranched structure is formed as the result of a grafting reaction.[1]

### Tensile testing

Figure 4 shows stress–strain curves for PP and simple blends, i.e. excluding PM. To demonstrate the initial elastic part of the diagram, it is magnified and presented in the inset. All the samples show similar behaviour. Stress increases linearly until it reaches its maximum at the yielding point. Then the stress decreases. At this point PP/PS (80:20) breaks. In contrast, the other samples can be strained further at almost constant stress. At an elongation around 250% a stress-hardening behaviour is distinguishable. Again stress

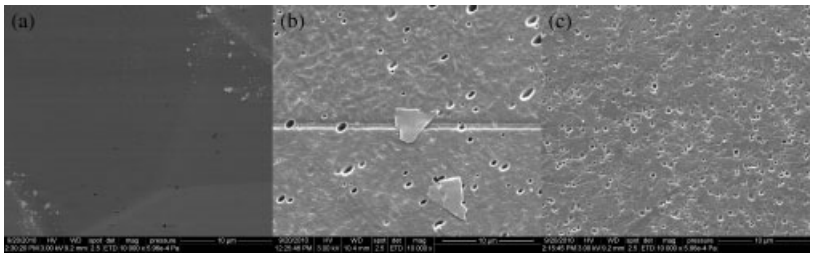


**Figure 3.** SEM images of (a) PP, (b) PP/PS (95:5) and (c) PP/PS/PM (90:5:5) after microtomy and etching.

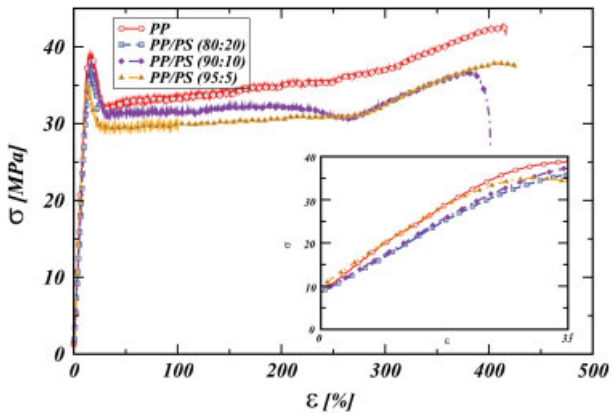


**Figure 4.** Stress–strain curves of PP and simple blends, i.e. excluding PM.

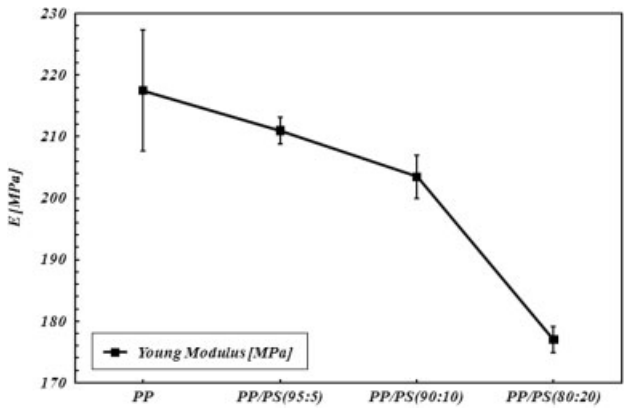


**Figure 5.** Elastic (Young's) modulus of non-reactively blended samples.

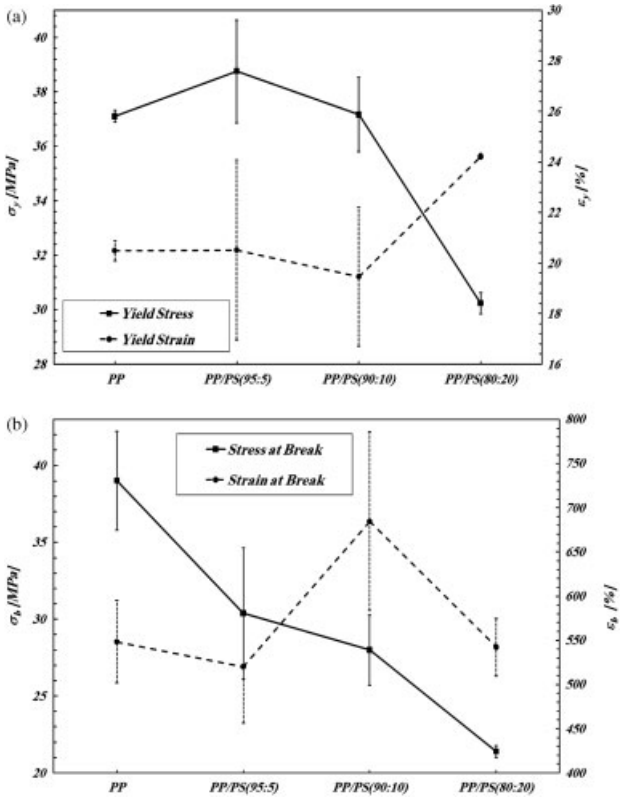


**Figure 6.** (a) Yield stress and strain and (b) stress and strain at break of non-reactively blended samples.

increases until the breaking point is reached. Breaking is sudden for all samples except PP/PS (90:10) which breaks less abruptly compared to the other samples.

The Young's moduli, *E*, obtained from the curves in Fig. 4, are shown in Fig. 5. *E* decreases with increasing PS content of the blends. The polar constituents of the interior parts of PS and also the existence of hydrophilic hydroxyl end groups on the surface of its molecules cause phase separation in the blends due to the non-polar hydrophobic structure of PP. The phase separation seen in the SEM image of PP/PS (95:5) supports the latter deduction.

Obviously with increasing PS content, aggregations are more likely to occur. Such heterogeneities are potential defects in mechanical tensile testing and as seen from Fig. 5, *E* decreases significantly with increasing PS in the blends. Also, the relatively small molecules of PS can play the role of a lubricating agent in solid state as hyperbranched molecules can also decrease the viscosity in melt or solution states.[1]

Figure 6 shows stress and strain values at yielding (Fig. 6(a)) and breaking (Fig. 6(b)) points. Yield stress, $\sigma_y$, and strain, $\varepsilon_y$, almost show no changes or a small decrease for samples that contain equal to or less than 10 wt%. Nevertheless, PP/PS (80:20) exhibits a significant reduction in $\sigma_y$ and an increase in $\varepsilon_y$. The ultimate properties are shown in Fig. 6(b). As a function of increasing PS, $\sigma_b$ decreases continuously, whereas $\varepsilon_b$ demonstrates an optimum value in PP/PS (90:10). These findings clearly show that PS has some kind of plasticizing effect in the blends and increases the flexibility. However, due to the formation of larger domains and bigger entities at greater amounts of PS, weakening heterogeneities become more probable, and this may be the reason for decreased $\varepsilon_b$ observed for PP/PS (80:20).

To determine how the reactively blended samples, i.e. those that contain PM, respond to mechanical loads and to study the effect of grafting reactions on the mechanical characteristics, PP/PS/PM (90:5:5) and PP/PS/PM (80:10:10) were investigated. Figure 7 shows



  

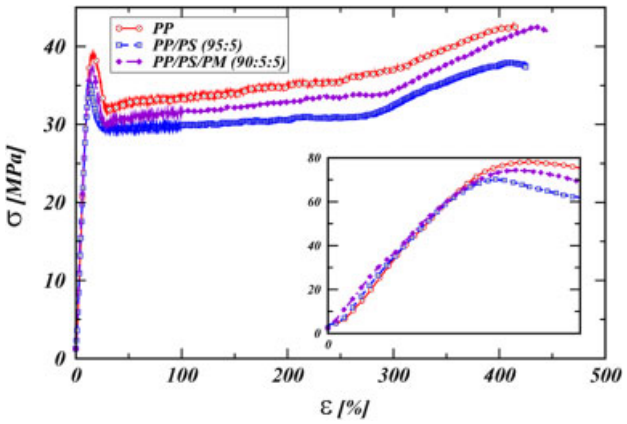


**Figure 7.** Stress–strain curves for PP, simple blend PP/PS (95:5) and reactive blended PP/PS/PM (90:5:5).

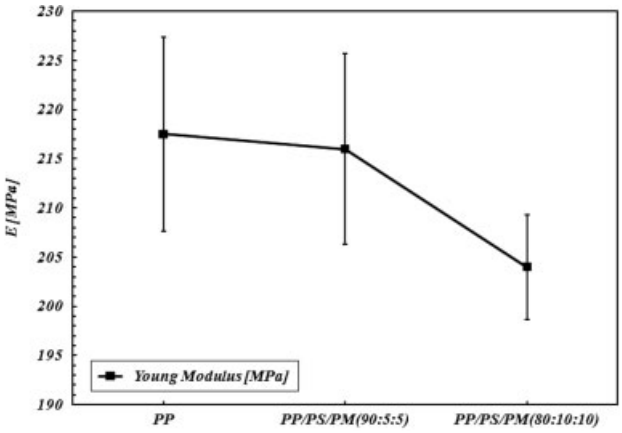


**Figure 8.** Elastic (Young's) modulus of PP and reactively blended samples.

stress–strain curves for PP, the simple blend PP/PS (95:5) and the reactively blended PP/PS/PM (90:5:5). Comparison with Fig. 4 shows that the behaviour is similar for these samples. In the elastic parts, stress increases linearly with increasing strain. After yielding, the stress decreases and then remains constant up to elongations around 250%. Then stress hardening occurs for all samples and ultimately the samples break abruptly.

Figures 8 and 9 illustrate $E$, $\sigma_y$, $\varepsilon_y$, $\sigma_b$ and $\varepsilon_b$ for PP and for reactively blended samples in which 3D crosslinked networks of nano-dendritic domains are formed. This has been studied previously.[1] Obviously PP/PS/PM (90:5:5) shows almost no difference in $E$ compared to PP whilst what is expected is that $E$ decreases due to the presence of two components that worsen the mechanical properties. Even for PP/PS/PM (80:10:10) the decrease in $E$ is not as strong as one would expect. Figure 9 depicts a slightly increased $\sigma_y$ and $\sigma_b$ and almost no changes in $\varepsilon_y$ and $\varepsilon_b$. Considering the unchanged value of $E$ for this blend, it has evidently become tougher. Such an enhancement in mechanical properties of reactively blended samples can most probably be attributed to the grafting reactions that lead to the formation of a crosslinked nanostructure of dendritic domains.[1] These domains can penetrate into the amorphous phase of the semi-crystalline structure of the PP matrix and act as a toughener. We can exclude that the observed increase of ductility is caused by orientation-induced crystallization of PP in the b-modification, because we have carried out wide-angle X-ray scattering measurements that show no change of the diffraction peaks as demonstrated in Fig. 10. Moreover, the low temperature, the very low strain rate and the absence of specific nucleating agents appear unfavourable concerning a generation of b-phase PP.

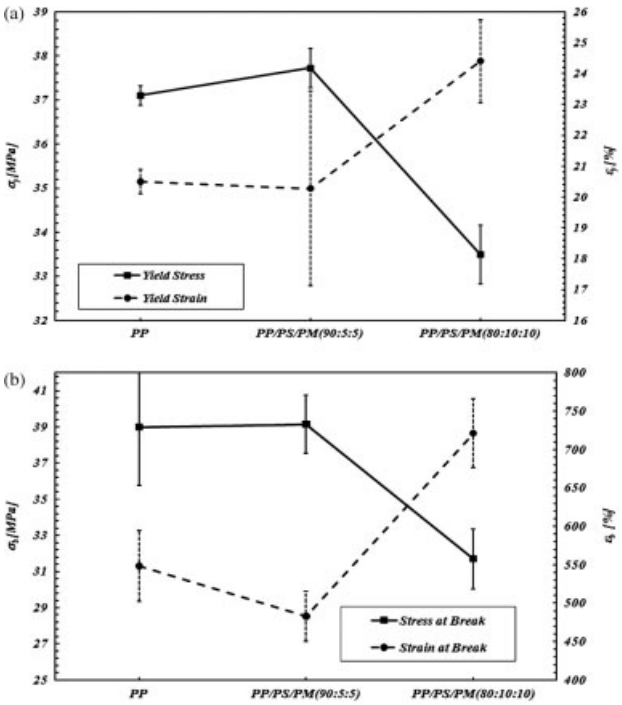


**Figure 9.** (a) Yield stress and strain and (b) stress and strain at break of reactively blended samples.

## SAXS patterns and CDFs

The mechanism that governs the mechanical behaviour discussed above was investigated using SAXS experiments. PP possesses a semi-crystalline morphology on which mechanical properties depend. Such structure begins to form when the melt is undercooled by more than 50 °C below the melting temperature.[21] This causes a strong sensitivity to additives in the matrix, in this case PS and PM. The semi-crystalline morphology itself and its behaviour were followed using SAXS. Figure 11 shows SAXS patterns and calculated CDFs both in 2D pseudo-colour and 3D surface plots for PP, PP/PS (95:5), PP/PS (90:10) and PP/PS/PM (90:5:5). All the samples exhibit discrete SAXS with distinct uniaxial orientation. Two-point patterns with peak maxima on the vertical axis ($s_3$, meridian, direction of melt flow in the bar, straining direction) are clearly observed. The SAXS pattern for PP also shows a second-order long-period reflection at larger angles that indicates a relatively regular arrangement of the crystallites. Second-order reflections are missing in the patterns of the other samples. Instead, an equatorial streak is observed that indicates the existence of domains that are extended in the straining direction, like crosshatched lamellae. The absence of second-order long-period reflections in the blend patterns shows that adding PS clearly distorts the stacking of crystalline domains in PP.

All the deductions from SAXS patterns in reciprocal space are more precisely visualized in real space after calculating the CDFs. The presence of lamellae oriented in the direction parallel to $s_3$ is deduced from the set of strong vertical streaks and from the corresponding modulation in the equatorial band of



  

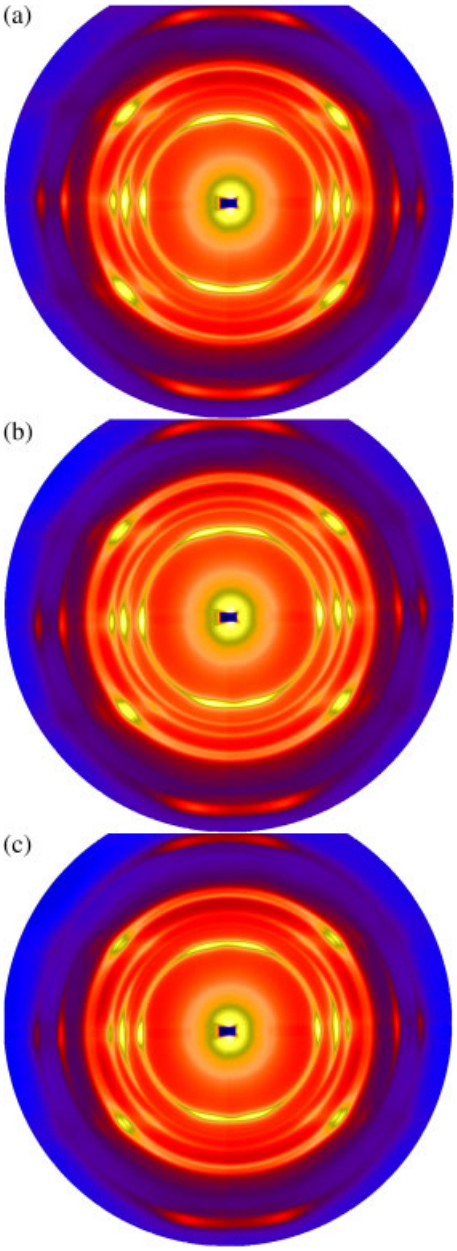


**Figure 10.** Wide-angle X-ray scattering patterns for (a) PP, (b) PP/PS (95:5) and (c) PP/PS/PM (90:5:5).

the CDF. The finding of two sets of lamellae that are oriented perpendicular to each other is compatible with a well-known peculiar architecture of PP nanostructure that is known as a mother–daughter crystal lamellar structure,[45–47] also called a crosshatching structure.[48,49] Utilizing these notions, it is possible to trace the nanostructural changes that occur as a consequence of the modification process both qualitatively and quantitatively. In the CDFs most distinguished are the layer-like peaks on the meridian which indicate stacks of alternating mother crystalline lamellae and amorphous layers of PP. The vertical bands describe the stacking of daughter crystal lamellae. The lateral extension of the layer peaks is a measure of the average lateral extension of the layers. Several separate reflections are gathered on the meridian which indicates that the thickness fluctuations of the lamellae are small and, for instance, in the case of PP at least three lamellae are correlated in each stack. The number of correlated lamellae in the stacks decreases to two for the other samples.[21]

For PP/PS (95:5) the pattern intensity reduces significantly both in meridional strip and equatorial band. The isotropic circle and the scattering of the second-order lamellae also vanish. This means, first of all, less orientation of mother crystal stacks and less vertical correlation through daughter crystal lamellae. Such consequences are simply deducible from the CDF image which demonstrates larger long period and wider vertical bands.

Comparing the CDFs from pure PP and PP/PS (90:10), the long period of the crystalline lamellae increases in both meridional and equatorial directions. In addition, a weak isotropic ring appears in the SAXS pattern of the blend that can most probably be attributed to the scattering by the dendritic polymer, PS, itself.

The scattering power $Q$ changes from $1.49 \times 10^{12}$ a.u. for pure PP to $1.17 \times 10^{12}$ a.u. for PP/PS (95:5) and $0.95 \times 10^{12}$ a.u. for PP/PS (95:10). We assume that this change is related to a decrease of crystallinity, although it is also possible to explain the finding by a successive reduction of the contrast between the amorphous and the crystalline phase in PP by incorporation of PS in the semi-crystalline PP. The probable reduction of the crystalline fraction in the matrix explains the mechanical deterioration of sample PP/PS (95:5) that is seen in macromechanical tensile tests. The reactively blended material PP/PS/PM (90:5:5) is different. In the SAXS pattern of PP/PS/PM (90:5:5) both the long-period peaks on the meridian and the intensity in the equatorial streak are much stronger than in the patterns of both PP/PS (95:5) and PP/PS (90:10). Even the isotropic ring is much more pronounced, and the scattering power $Q$ is increased to $1.27 \times 10^{12}$ a.u. Overall, the semi-crystalline nanostructure of this sample appears more similar to that of PP than to that of the non-reactively blended materials. Concerning the mechanical properties, a corresponding similarity has already been reported in the previous section. Definitely responsible are the crosslink domains introduced by the dendritic polymer and resulting from the surface modification and grafting reaction. Such domains are smaller in size and distributed more evenly in the PP matrix due to manipulated amphiphilic characteristic as a result of the surface modification. Altering the hydrophilic hydroxyl groups with the hydrophobic PP chains increases miscibility. These smaller domains penetrate into the amorphous phase in general, i.e. in both the amorphous layers constrained in the semi-crystalline stacks and the free amorphous matrix outside the stacks.[50] This tends to evidence that the compactness of the structure is less affected and as a consequence that less disordering of the crystal orientations occurs. In addition, the crosslinked networks of the domains are now more capable of scattering because of the 3D structure and higher electron density. That is why a stronger isotropic ring appears in the pattern. The CDF image confirms these findings which are also in good agreement with the mechanical results.

### SAXS patterns and CDFs as a function of strain

Figure 12 shows SAXS patterns recorded while the samples were subjected to mechanical load and the CDFs calculated from them.

A general behaviour can be recognized in all three loaded samples. At the very beginning of straining and low elongation, the intensity of the scattering pattern increases without any variation in the shape. Then as straining continues and elongation increases, the meridional scattering and the equatorial streak gradually disappear. In the end the pattern turns into an equatorial streak and no meridional scattering remains. Apparently, at elongations before the yielding point (i.e. $\varepsilon = 0.05$ for PP, $\varepsilon = 0.08$ for PP/PS



  

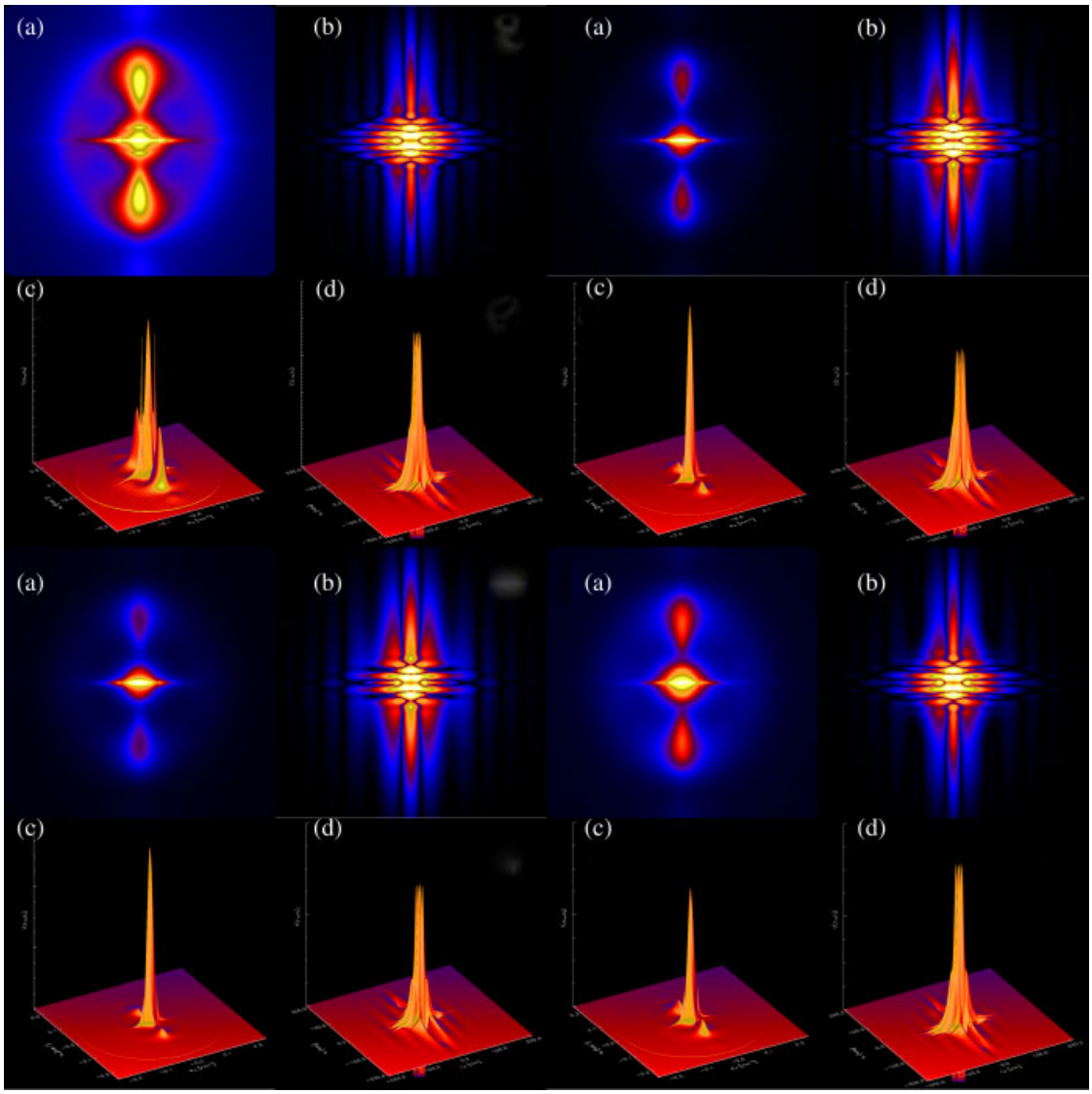


**Figure 11.** (a) SAXS patterns in 2D and (c) 3D views and (b) calculated CDFs in 2D and (d) 3D views of PP (top left), PP/PS (95:5) (top right), PP/PS (90:10) (bottom left) and PP/PS/PM (90:5:5) (bottom right).

(95:5) and $\varepsilon = 0.09$ for PP/PS/PM (90:5:5)), there is no destructive rearrangement of the crystal lamellae and applying load only orients the tilted stacks that consequently leads to an increase in meridional scattering. Continuing the straining causes the mother crystal lamellae to break into pieces and daughter lamellae to tear down. This results in vanishing and changing of the scattering pattern as is obvious in Fig. 12. Later on along with development of yielded area, fibrils are made parallel to the direction of stretching and an equatorial streak resulting from the fibrils emerges in the pattern.

The calculated CDFs of these patterns precisely visualize the aforementioned explanations in real space. Figure 13 shows the deformation of the semi-crystalline stacks in the materials on the nanometre scale, i.e. the nanodeformation, $\varepsilon_{Nano}$, together with the macromechanical parameters. $\varepsilon_{Nano}$ is been extracted from the position of the long-period peak on the negative face of the CDF images. The true macroscopic strain is calculated by measuring the displacements of fiducial marks on the samples.[50] Figure 14 shows that, for PP, $\varepsilon_{Nano}/\varepsilon_{Macro} < 1$ is valid both before and after the yielding point. It is also clear from Fig. 14 that $\varepsilon_{Nano}/\varepsilon_{Macro}$ increases as the straining continues. PP/PS (95:5) and PP/PS (90:10) demonstrate similar behaviour as both show ratios greater than that at the very beginning of straining and then the values decrease markedly. The mentioned relaxation in $\varepsilon_{Nano}$ occurs for both samples as well. The reactively grafted sample PP/PS/PM (90:5:5) seems to be more like PP as $\varepsilon_{Nano}/\varepsilon_{Macro}$ is smaller than unity and right after passing the yielding point a relaxation occurs for $\varepsilon_{Nano}$. To explain why $\varepsilon_{Nano}/\varepsilon_{Macro}$ is almost always smaller than unity one should turn to the origins of nano- and macrodeformation. Nanodeformation is in fact deformation of the amorphous part sandwiched between two crystal lamellae. It is obtained from peak position displacement in the CDF images which is in fact displacement of crystal lamellae. However, macrodeformation arises from stretching the free amorphous part in which crystal stacks are distributed. Applying mechanical load causes straining of both amorphous parts. At low elongation both parts deform similarly, while at higher strain the free amorphous part proves to be more extensible than the constrained one. This is because the sandwiched part between two crystal lamellae acts somehow as a fixed spring with higher modulus compared to



  

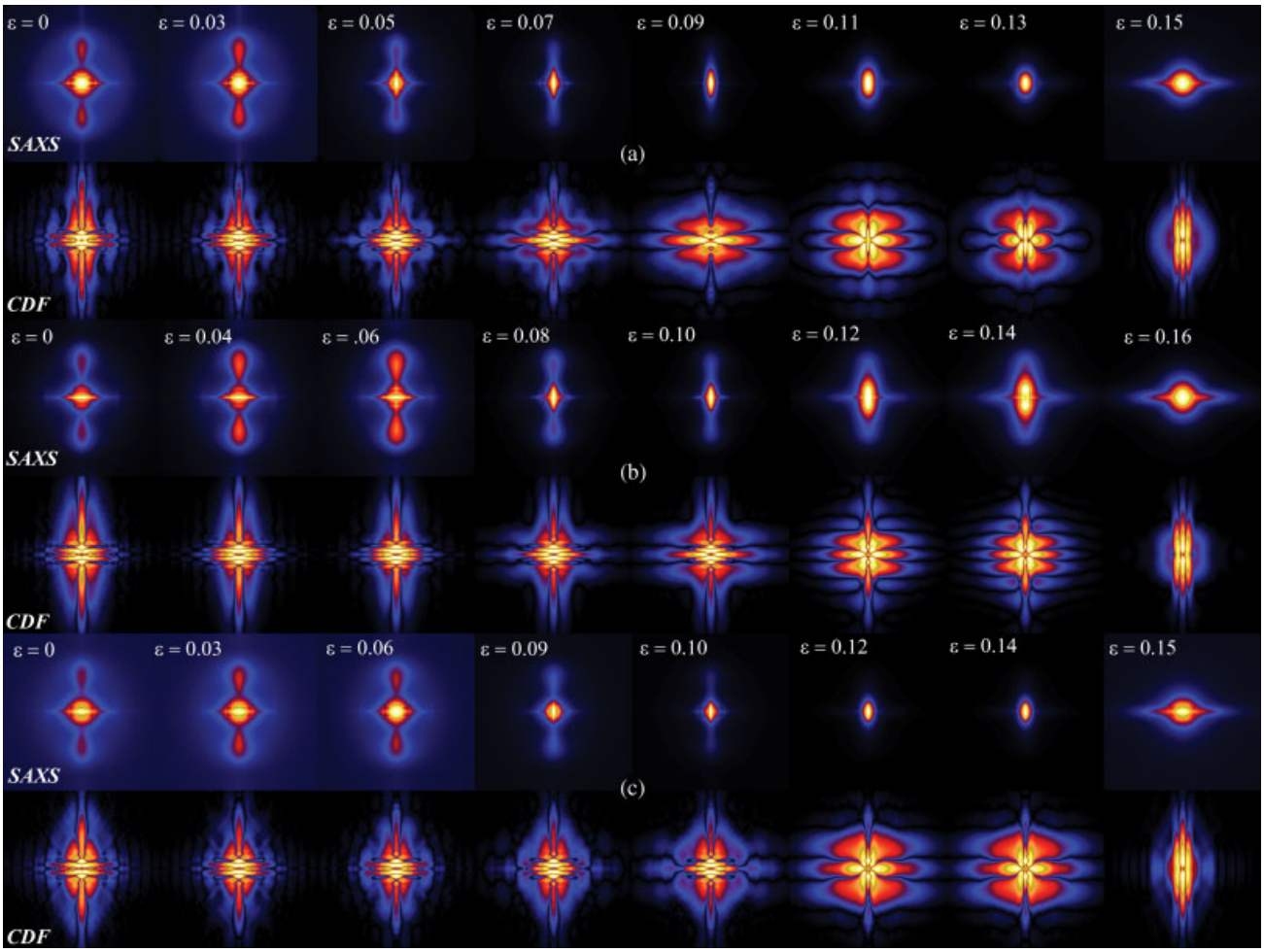


**Figure 12.** SAXS patterns and calculated CDFs obtained from (a) PP, (b) PP/PS (95:5) and (c) PP/PS/PM (90:5:5) under mechanical loads.

the free part according to tie molecules theory.[51–54] This also has been described by Tang *et al.*[55] According to their findings the extensibility of the amorphous part between the crystalline domains is limited. As the macroscopic deformation increases further, microfibrils originated from the stacks of lamellae begin to slip past each other, but the distance between the crystalline grains remains almost constant. This slipping process results in the macroscopic strain. That is why $\varepsilon_{Nano}/\varepsilon_{Macro}$ gradually decreases as elongation increases. When the yielding point is reached, failures in the free amorphous part occur that release the stresses from the connected sandwiched amorphous parts. This leads to resilience of the sandwiched amorphous regions and the corresponding retraction is observed in the diagrams by a reduction of $\varepsilon_{Nano}$. Thereafter, as stretching continues, the crystalline grains are destroyed and no distinguishable fractions of amorphous phase exist anymore.

To compare the deformation behaviour of the samples more specifically, $\varepsilon_{Nano}$ and $\varepsilon_{Macro}$ of PP, PP/PS (95:5) and PP/PS/PM (90:5:5) are plotted together in Fig. 15. The applied stress is also shown for PP and PP/PS/PM (90:5:5). The left-hand panel shows deformation of PP compared with PP/PS (95:5). Although macrodeformation is nearly similar especially at lower elongation, $\varepsilon_{Nano}$ shows different trends. At first, PP/PS (95:5) shows greater values for nanodeformation until stress reaches its maximum. Afterwards, $\varepsilon_{Nano}$ for PP dominates and remains higher up to the end of the experiment. The same occurs for PP/PS/PM (90:5:5) as can be seen from the right-hand panel in Fig. 15. As explained in the literature,[1] introducing dendritic polymers into a PP matrix causes chain entanglements to decrease. This is somewhat seen in static measurements as the tight crosslinked nanocrystalline structure of PP becomes less compressed, and the long period of the crystal lamellae increases when PS is incorporated into the matrix. Considering this lubricating effect of PS, the higher $\varepsilon_{Nano}$ for PS-containing blends is explainable. Chain mobility even between the lamellae, the sandwiched part, is more likely for these blends. Soon after the yield stress is reached at which structure failure happens, $\varepsilon_{Nano}$ for PP becomes higher compared to that for the other two samples. Higher chain mobility of the PS blended samples eases the returning of spring-like sandwiched parts back together as a result of stress release. Thus, $\varepsilon_{Nano}$ for PP/PS (95:5) and PP/PS/PM (90:5:5) becomes smaller and experiences a more significant relaxation. The deteriorating macromechanical properties, as seen before, is in good agreement with these findings. It evidences that the higher the nanodeformation, the smaller the elastic modulus. Also the more similar deformation behaviour of PP and PP/PS/PM (90:5:5) means that these two materials must possess the same mechanical properties as was shown previously. The latter is another confirmation of the good correlation of macromechanical properties and nanodeformation behaviour.



  

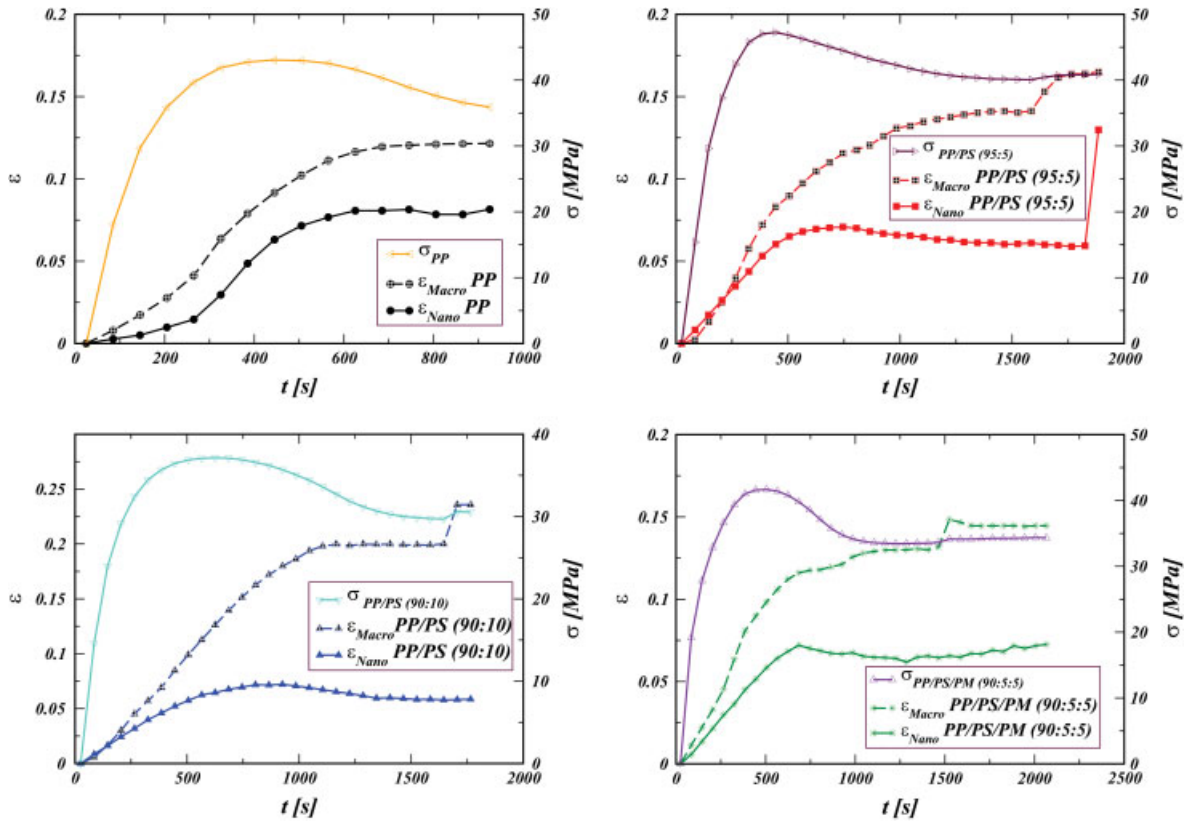


**Figure 13.** Nanodeformation, $\varepsilon_{Nano}$, true strain, $\varepsilon_{Macro}$, and applied stress, $\sigma$, of PP, PP/PS (95:5), PP/PS (90:10) and PP/PS/PM (90:5:5).

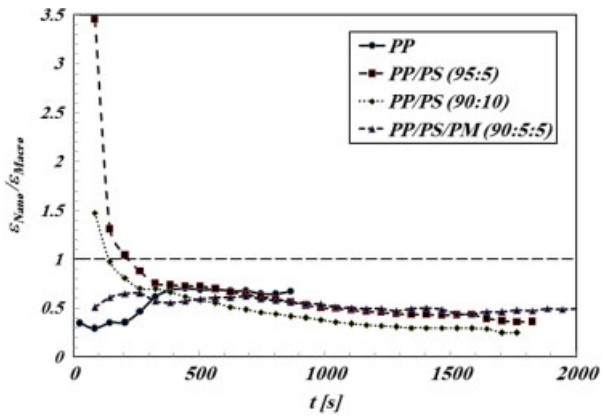


**Figure 14.** $\varepsilon_{Nano}/\varepsilon_{Macro}$ ratios during application of mechanical load.

To understand the effect of grafting reaction, $\varepsilon_{Nano}$ and $\varepsilon_{Macro}$ for PP/PS (95:5) and PP/PS/PM (90:5:5) are plotted together in Fig. 16. This shows that macrodeformation for grafted sample, i.e. including PM, is higher while it shows smaller nanodeformation. It was explained previously that the outcome of grafting reaction is a 3D crosslinked network of dendritic domains. Parts of such structures as stronger springs with higher constant coefficient are supposed to diffuse into the crystal lamellae and locate between the sandwiched amorphous part. This surely leads to more difficult deformations at the nanoscale, as clearly demonstrated in Fig. 16.

The same reasoning rationalizes milder relaxation for the grafted sample, as the mentioned stronger springs will prevent lamellae receding on their way back together. The expected structure is shown schematically in Fig. 17.

## CONCLUSIONS

PP was modified by the use of a poly(ester amide)-based hyperbranched polymer. Two different approaches, simple blending and reactive blending, were exploited and macromechanical characteristics and nanostructural parameters were studied. It was found that simple blending of the hyperbranched polymer deteriorates mechanical behaviour compared to that of neat PP; however, reactive blending compensates this decrease up to that of the blank sample, PP. Following these finding at the nanoscale with the aid of time-resolved SAXS measurements demonstrated good correlation between macromechanical behaviour and nanostructural parameters as the samples with similar nanostructures showed nearly the same macromechanical parameters. Different rationalizations were offered to explain these findings and a schematic structure of the reactively blended sample was presented to gain a better understanding of what happens at the nanoscale.

## ACKNOWLEDGEMENTS

The authors thank the Hamburg Synchrotron Radiation Laboratory (HASYLAB) for beam time granted. Frank Derks from DSM Hybrane is acknowledged for kindly providing the hyperbranched polymer. The support from Professor Dr Gerrit A Luinstra from the TMC Department at the University of Hamburg is appreciated.



  

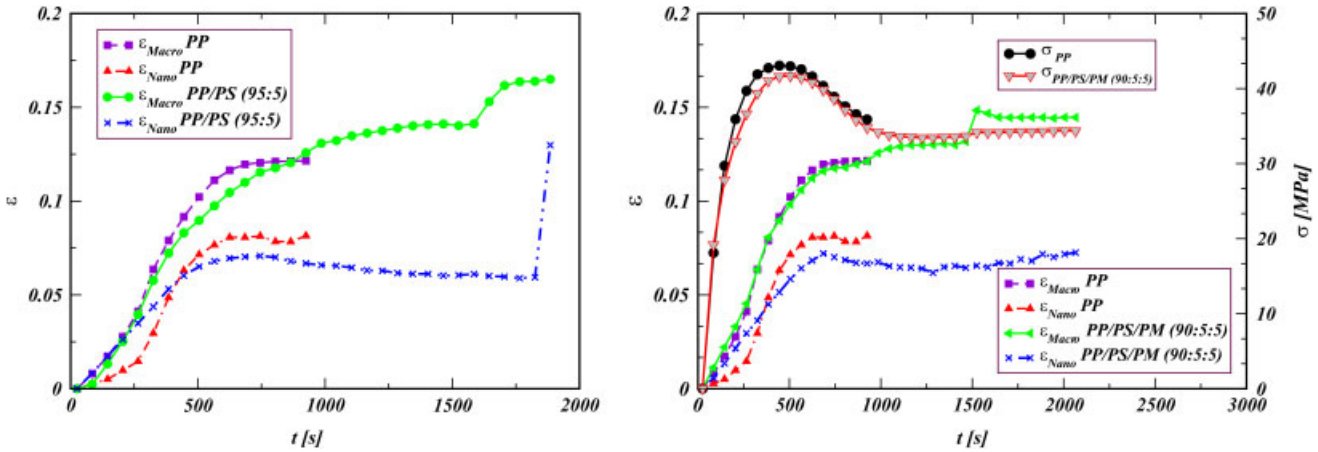


**Figure 15.** Comparison of nano- and macrodeformation of samples.

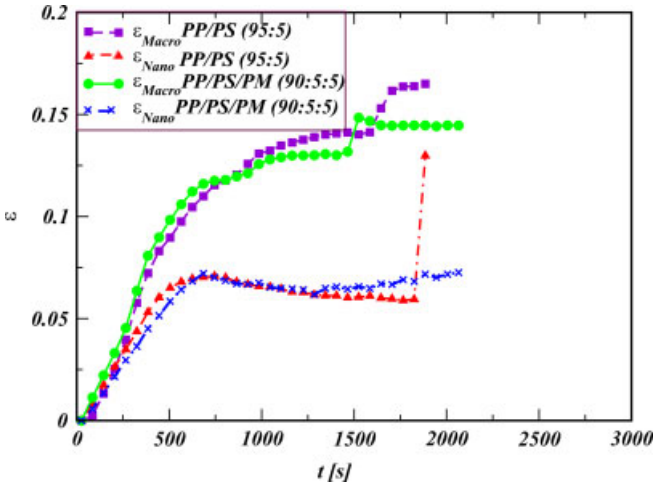


**Figure 16.** Comparison of nano- and macrodeformation of non-grafted and grafted samples.

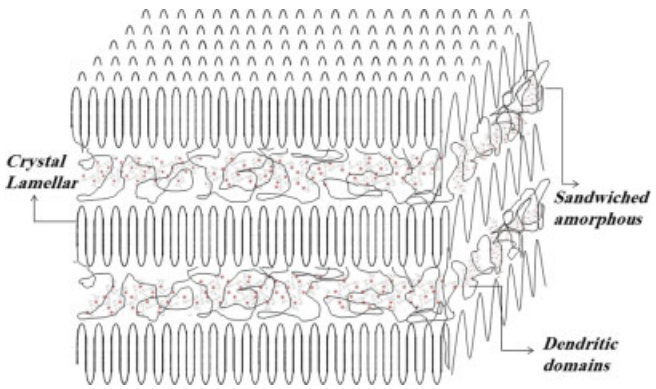


**Figure 17.** Schematic of crystalline nanostructure of reactively blended (grafted) sample.

## REFERENCES


1 Sari MG, Moradian S, Bastani S and Stribeck N, *J Appl Polym Sci* **124**:2449–2462 (2011).
2 Ujhelyiova A, Bolhova E, Oravkinova J, Tino R and Marcincin A, *Dyes Pigments* **72**:212–216 (2007).
3 Xu G, Shi W, Hu P and Mo S, *Eur Polym J* **41**:1828–1837 (2005).
4 Karian HG, *Handbook of Polypropylene and Polypropylene Composites*, 2nd edition. Marcel Dekker, New York (2003).
5 Tripathi D, *Practical Guide to Polypropylene*. Rapra Technology, Shrewsbury (2002).
6 Tao G, Gong A, Lu J, Sue HJ and Bergbreiter DE, *Macromolecules* **34**:7672–7679 (2001).
7 Maier C and Calafut T, *Polypropylene: The Definitive User's Guide and Databook*. Plastics Design Library, New York (1998).
8 Akrman J and Přikryl J, *J Appl Polym Sci* **66**:543–550 (1997).
9 Akrman J and Přikryl J, *J Appl Polym Sci* **62**:235–245 (1996).
10 Moore EP, *Polypropylene Handbook*. Carl Hanser Verlag, Munich (1996).
11 Miyazaki K, Tabata I and Hori T, *Color Technol* **128**:51–59 (2012).
12 Miyazaki K, Tabata I and Hori T, *Color Technol* **128**:60–67 (2012).
13 Asiaban S and Moradian S, *J Appl Polym Sci* **123**:2162–2171 (2012).
14 Seves A, De Marco T, Siciliano A, Martuscelli E and Marcandalli B, *Dyes Pigments* **28**:19–29 (1995).
15 Yaman N, Özdoğan E, Seventekin N and Ayhan H, *Appl Surf Sci* **255**:6764–6770 (2009).
16 Cui ZH, Zhang SF and Yang JZ, *Chinese Chem Lett* **18**:1145–1147 (2007).
17 Asiaban S and Moradian S, *Dyes Pigments* **92**:642–653 (2012).
18 Tavanaie MA, Shoushtari AM and Goharpey F, *J Clean Prod* **18**:1866–1871 (2010).
19 Burkinshaw SM, Froehling PE and Mignanelli M, *Dyes Pigments* **53**:229–235 (2002).
20 Burkinshaw SM, Mignanelli M, Froehling PE and Bide MJ, *Dyes Pigments* **47**:259–267 (2000).
21 Stribeck N, Zeinolebadi A, Sari MG, Botta S, Jankova K, Hvilsted S, *et al*., *Macromolecules* **45**:962–973 (2012).
22 Compostella M, Coen A and Bertinotti F, *Angew Chem* **74**:618–624 (1962).
23 Norton DR and Keller A, *Polymer* **26**:704–716 (1985).
24 Olley RH and Bassett DC, *Polymer* **30**:399–409 (1989).
25 Stribeck N, Nöchel U, Funari S and Schubert T, *J Polym Sci Polym Phys* **46**:721–726 (2008).
26 Stribeck N, *X-Ray Scattering of Soft Matter*. Springer-Verlag, Berlin (2007).
27 Stribeck N, *J Appl Crystallogr* **34**:496–503 (2001).
28 Stribeck N, in *Nano- and Micromechanics of Polymer Blends and Composites*, vol. 1, ed. by Karger-Kocsis J and Fakirov S. Hanser Verlag, Munich, pp. 269–300 (2009).
29 Denchev Z, Dencheva N, Funari SS, Motovilin M, Schubert T and Stribeck N, *J Polym Sci B: Polym Phys* **48**:237–250 (2010).
30 Stribeck N, *J Appl Crystallogr* **34**:496–503 (2001).
31 Stribeck N and Wutz C, *Macromol Chem Phys* **203**:328–335 (2002).
32 Stribeck N, Androsch R and Funari SS, *Macromol Chem Phys* **204**:1202–1216 (2003).
33 Stribeck N, Fakirov S, Apostolov AA, Denchev Z and Gehrke R, *Macromol Chem Phys* **204**:1000–1013 (2003).
34 Stribeck N and Fakirov S, *Macromolecules* **34**:7758–7761 (2001).
35 Stribeck N, *Fibres Text E Eur* **11**:33–36 (2003).
36 Stribeck N, in *Condensation Thermoplastic Elastomers*, ed. by Fakirov S. Wiley-VCH, Weinheim, pp. 197–225 (2005).
37 Stribeck N, *Anal Bioanal Chem* **376**:608–614 (2003).




  

38 Stribeck N, Camarillo AA, Cunis S, Bayer RK and Gehrke R, *Macromol Chem Phys* **205**:1445–1454 (2004).
39 Debye P and Bueche AM, *J Appl Phys* **20**:518–525 (1949).
40 Porod G, *Colloid Polym Sci* **124**:83–114 (1951).
41 Vonk CG, *J Appl Crystallogr* **6**:81–91 (1973).
42 Baltaá Calleja FJ and Vonk CG, *X-Ray Scattering of Synthetic Polymers*. Elsevier, Amsterdam (1989).
43 Ruland W, *Colloid Polym Sci* **255**:417–427 (1977).
44 Vonk CG, *Colloid Polym Sci* **257**:1021–1032 (1979).
45 Meille SV, Briickner S and Porzios W, *Macromolecules* **23**:4114–4121 (1990).
46 Auriemma F and De Rosa C, *Macromolecules* **39**:7635–7647 (2006).
47 Li H, Sun X, Wang J, Yan S and Schutz JM, *J Polym Sci B: Polym Phys* **44**:1114–1121 (2006).
48 Zhu X, Melian C, Dou Q, Peter K, Demco DE, Möller M, *et al*., *Macromolecules* **43**:6067–6074 (2010).
49 van der Meer DW, Milazzo D, Sanguineti A and Vancso GJ, *Polym Eng Sci* **45**:458–468 (2005).
50 Stribeck N, Zeinolebadi A, Sari MG, Frick A, Mikoszek M and Botta S, *Macromol Chem Phys* **212**:2234–2248 (2011).
51 Weiner JH and Berman DH, *Macromolecules* **17**:2015–2018 (1984).
52 Stribeck N, Sapoundjieva D, Denchev Z, Apostolov AA, Zachmann HG, Stamm M, *et al*., *Macromolecules* **30**:1329–1339 (1997).
53 Stribeck N, Fakirov S and Sapoundjieva D, *Macromolecules* **32**:3368–3378 (1999).
54 Flores A, Pietkiewicz D, Stribeck N, Roslaniec Z and Baltá Calleja FJ, *Macromolecules* **34**:8094–8100 (2001).
55 Tang Y, Jiang Z, Men Y, An L, Enderle HF, Lilge D, *et al*., *Polymer* **48**:5125–5132 (2007).

  